



Heat transfer correlations of refrigerant falling film evaporation on a single horizontal smooth tube

Pu-Hang Jin, Zhuo Zhang, Ibrahim Mostafa, Chuang-Yao Zhao, Wen-Tao Ji, Wen-Quan Tao*

Key Laboratory of Thermo-Fluid Science and Engineering of MOE, School of Energy and Power Engineering, Xi'an Jiaotong University, Xi'an 710049, PR China

ARTICLE INFO

Article history:

Received 7 June 2018

Received in revised form 12 November 2018

Accepted 10 December 2018

Available online 19 December 2018

Keywords:

Falling film evaporation

Nucleate boiling

Single horizontal plain tube

Heat transfer correlations

ABSTRACT

Falling film evaporation heat transfer of R134a and its potential substitutes R290 and R600a outside a single horizontal plain tube is experimentally investigated, and the effects of the saturation temperature, film flow rate and heat flux on heat transfer coefficient are studied. Heat transfer performance of R290 is slightly superior than that of R134a, while R600a is inferior than that of R134a. The threshold film Reynolds number is determined to separate the variation trend of HTC with film Reynolds number into full wetting and partial dryout regimes. Increase of heat flux benefits the heat transfer in both full-wetting and partial dry-out regimes. New heat transfer correlations based on the present data and data for R32 and R1234ze(E) in the authors' group are suggested for two regimes. The correlation for full wetting regime fits 96.7% of the total 542 correlated data within $\pm 30\%$ while fits 73.4% of the total 289 data in references from -30% to $+15\%$, the correlation for partial dryout regime fits 97.5% of the total 162 correlated data within $\pm 30\%$ while fits 76.8% of the total 95 data from references within $\pm 30\%$.

© 2018 Published by Elsevier Ltd.

1. Introduction

Falling film evaporator is a type of shell-tube evaporator with quite a long history and widely used in petrochemical industry, food processing, desalination process, OTEC (ocean thermal energy conversion) system and ORC (organic Rankine cycle) system. It is known as a potential substitute to pool boiling evaporator in a water chiller or heat pump system due to its several intrinsic advantages over pool boiling like less refrigerant charge, smaller size, smaller temperature difference of heat transfer and easier oil removal, etc. Despite the fact that many studies have been performed, we are still lack of satisfied heat transfer correlations, not mentioned to design data of horizontal tube-bundle falling film evaporator. Up to now we even don't have a well-accepted heat transfer correlation for falling film evaporation on horizontal single smooth tube of refrigerants.

Recent years, numerous investigators have paid their attention on falling film evaporation (FFE) over horizontal tubes. Moeykens [1] tested a plain-surface tube, two condensation-enhanced tubes, two boiling-enhanced tubes, and two finned tubes in a multi-tube falling film evaporation test facility with R134a. He found that the two enhanced condensation surfaces performed best among tubes tested under the same working conditions. Roques and Thome [2],

Habert and Thome [3] and Christians and Thome [4] extended the existing database of falling film evaporation HTCs with new refrigerants (R236fa) and structured surfaces (TurboB-5, Gewa B-5, High Flux, etc.). Local heat transfer coefficients are obtained by the modified Wilson Plot method. Also they proposed new prediction method for predicting onset of dryout and heat transfer coefficients for commercial enhanced boiling tube. Ji et al. [5] and Zhao et al. [6–8] studied the effect of vapor flow, enhanced structure and tube bundle on heat transfer characteristics of FFE. Vapor flowing upward with a velocity of 0–3.1 m/s and vapor flowing crossward with a velocity of 0–2.4 m/s are investigated in their study, at higher vapor velocity, the vapor will have a considerable shear stress on the flowing thin liquid film and even disrupt it to induce some dryout area. Condensation enhanced tube is found to outperform three enhanced boiling tubes tested. Average heat transfer coefficient of the tube bundle decreases with increase of heat flux, higher saturation temperature benefits the heat transfer performance. More comprehensive reviews on different aspects of FFE can be found in Fernández-Seara and Pardiñas [9] and Abed et al. [10].

In this paper focus will be concentrated on heat transfer on single smooth tube. Falling film evaporation on a single smooth tube is the very basic topic in this research field, and several researchers have suggested empirical correlations to predict heat transfer coefficients outside single smooth tube [11–17]. Expression of these

* Correspondent author.

E-mail address: wqtao@mail.xjtu.edu.cn (W.-Q. Tao).

Nomenclature

A	area, m ²
D	diameter of tube, mm
FFE	falling film evaporation
h	heat transfer coefficient/HTC, W·m ⁻² ·K ⁻¹
k	overall heat transfer coefficient, W·m ⁻² ·K ⁻¹
L	test length of tube, mm
PB	pool boiling
q	heat flux, kW·m ⁻²
R	thermal resistance, m ² ·K·W ⁻¹
r	latent heat, J·kg ⁻¹
Re_f	film Reynolds number
T	temperature, °C
V	velocity of water, m·s ⁻¹

Greeks

Δ	variable differential
Γ	liquid film flow rate on one side of the tube per unit length, kg·m ⁻¹ ·s ⁻¹
ϕ	heat transfer rate, W
μ	dynamic viscosity, kg·m ⁻¹ ·s ⁻¹

Subscripts

c	condensation
e	evaporation
f	fouling
G_{ni}	Gnielinski equation
l	liquid refrigerant
v	vapor refrigerant
LMTD	logarithmic mean temperature difference
i	inside of tube
m	mean
o	outside of tube
p	pump
r	reference
sat	saturation
w	wall
in	water inlet
out	water outlet
pre	prediction
exp	experiment

correlations and their working conditions are summarized in Table 1.

Danilova and co-workers [11] proposed correlations based on experimental results with the refrigerants of R-22, R-12 and R-113 in a tube bank. Two correlations are proposed for the top-most tube and the rest of tubes respectively by Fujita and Tsutsui [12] based on the experimental data of R-11. Full wetting conditions are assumed in their heat transfer correlations and an empirical relation is established between heat flux and threshold film Reynolds number for inception of film breakdown. Tests are conducted under quite a low heat flux from 0.5 to 15 kW/m² dominated by evaporation without boiling. Ribatski and Thome [13] suggested an objective criterion to predict the onset of dryout and a correlation to predict the HTCs under dryout conditions as well as non-dryout conditions by defining an apparent wet ratio. In their study, test was conducted in a tube bundle with R134a while data of the top tube is not taken as the data base to obtain the correlations. The total heat transfer flow are divided into two parts, wet regions dominated by nucleate boiling and dry regions dominated by natural convection, to calculate the average heat transfer coefficient of outer copper surface. A new superposition model of falling film evaporation on horizontal tubes is proposed by Chien and his co-workers [14–16]. The new superposition model in [14] accounts for the falling film evaporation heat transfer coefficient by nucleate boiling coefficient and two-phase convection coefficient respectively. The suppression factor for nucleate boiling is correlated based on the experimental data of five refrigerants, that is R134a, R22, R123, R141b and R11. In [15], the model is established for conditions with and without boiling separately based on the experimental data of R245fa. Different from the method used in [14], falling film convection coefficient is correlated under non-boiling condition rather than adopted from Alhuisseini et al. [18]. Boiling suppression factor is correlated by the new experimental data of R245fa. While in [16], the empirical boiling suppression factor is refitted with new test data of R134a. Most recently, correlations presented by Zhao et al. [17] achieve quite success in predicting not only their own data but also data for several other refrigerants from references despite the fact that their correlations are only based on the data of R134a. Effect of tube diameter on the heat transfer coefficient is also taken into

consideration. Heat transfer coefficient is predicted for partial dry-out regime and full wetting regime respectively which are separated by a threshold film Reynolds number.

Since the falling film evaporation heat transfer is a very complicated process and affected by many factors, so far it's hard to solve or simulate it accurately with theoretical or numerical methods. Empirical correlations are the most useful tool for falling film evaporator design. As the first step the heat transfer community should have a well-accepted correlation for horizontal smooth tube such that it can be used as a reference to check the test data for later experimental study, like cooper correlation [19] for pool boiling test. The major purpose of this study is to obtain a new correlation based on the previous studies with a better accuracy and wider applicability. In this study, apart from the experimental data conducted by authors for three refrigerants (R134a, R290 and R600a), data of other two refrigerants (R32 and R1234ze(E)) from references [20,21] are also employed to extend the database on which new heat transfer correlations will be established. R290, R600a and R1234ze(E) are three potential substitutes to R134a because of their very low GWP (global warming potential) despite that fact that R290 and R600a have a high flammability, and R32 is an indispensable ingredient in many mixture refrigerants which may achieve a balance between working efficiency and GWP value. Thermo-physical properties of the working fluids are given in Table 2.

In the next part, the experiment system is briefly described, followed by a description of data reduction method and uncertainty analysis, then experimental results and empirical correlations are analyzed and discussed, finally some conclusions are drawn.

2. Experimental system

2.1. Experimental facility

In this section, the experimental apparatus and measurement instruments are introduced. As shown in Fig. 1, the experimental system consists of three major circulation loops which are heating (hot) water circuit, chilling (cold) water circuit and refrigerant circuit. Liquid refrigerant is stored at the bottom of the condenser (reservoir). During operation, liquid refrigerant is pumped to the

Table 1
Heat transfer correlations of falling film evaporation on single horizontal plain tube.

Correlation	Fluids/ D_o ,mm	Working conditions q , kW/m ²
[11] $h_o/\lambda_i(\sigma/(g(\rho_l - \rho_v)))^{1/2} = 1.32 \times 10^{-3} ((q/(r\rho_l v_i))(\sigma/(g(\rho_l - \rho_v))))^{0.22}(p_{sat}/\sigma((\sigma/g(\rho_l - \rho_v))^{1/2})^{0.72}) Pr^{0.48}$	R-22, R-12 and R-113/18.0	Re: 135–2500 q: 0.5–25
[12] $Nu = (Re_f^{-2/3} + 0.008Re_f^{0.3} Pr^{0.25})^{1/2}$ for the first tube $Nu = (Re_f^{-2/3} + 0.01Re_f^{0.3} Pr^{0.25})^{1/2}$ for the rest of tubes where $Nu = h_o(v^2/g)^{1/3}/\lambda_i$	R11/25.0	Full wetting/No boiling Re: 10–2000 q: 0.5–15
[13] $h_o = 4200Pr_{red}^{0.22} q^{0.38} M^{-0.5} Ra^{0.2} (0.0024 Re^{0.91}) + h_{dry}(1 - 0.0024 Re^{0.91})$	R134a/19.05	Partial dryout Re: 157–2500
[14] $h_o = (0.185 + 56.21We^{0.4531}/(Bo^{0.687} Re^{1.3078})) h_{nb} + h_{cv}$	R-123, R-22, R-11, R-134a and R-141b/12.7–19.5	Pr: 2.54–5.9 q: 2–100 Re: 115–372 Pr: 6.26–7.15 We: $1.65-16.8 \times 10^{-4}$ Bo: 0.044–0.473 Re: 184–750 Pr: 3.45–3.74 We: $2.3-2.9 \times 10^{-3}$ Bo: 0.042–0.469 Re: 255–1495 Bo: $0.42-21.4 \times 10^{-2}$ Pr: 3.40–4.25 We: $0.93-45.13 \times 10^{-4}$ Re: 250–2697, Bo: $0.52-25.88 \times 10^{-2}$ Pr: 3.56–3.83 We: $0.82-99.58 \times 10^{-4}$
[15] $h_o = (0.0152We^{0.2833} Re^{1.2536} Bo^{1.1789}) h_{nb} + h_{cv}$	R245fa/19.0	
[16] $h_o = (56.13We^{0.5878} Re^{0.2457}/Bo^{0.1798}) h_{nb} + h_{cv}$	R134a/19.0	
[17] $Nu = 4.64 \times 10^{-3} Re^{1.51} Bo^{0.43} Pr^{0.15} We^{-0.45}$ (Partial dryout) $Nu = 3.58 \times 10^{-9} Re^{2.89} Bo^{0.37} Pr^{0.2} We^{-1.13}$ (Full wetting)	R134a/16.0, 19.05 and 25.35	

Table 2
Thermo-physical properties of the working fluids.

Fluid Type	R134a	R290	R600a	R32	R1234ze(E)		
$T_{sat}/^{\circ}C$	6	6	10	6	6		
P_{sat}/MPa	0.3620	0.5675	0.6366	0.1932	0.2206	0.9811	0.2686
$\rho_l/kg/m^3$	1274.7	520.36	514.73	573.63	568.92	1034.2	1222.4
$\rho_v/kg/m^3$	17.717	12.315	12.315	5.1749	5.867	26.714	14.402
$\lambda_i/W/m-K$	0.089367	0.10292	0.10093	0.096311	0.094788	0.14053	0.080877
$c_p/kJ/kg-K$	1.3581	2.5399	2.5733	2.3155	2.3382	1.7795	1.3322
$r/kJ/kg$	192.95	366.26	360.28	348.58	344.63	305.66	180.30
$\mu/\mu Pa-s$	246.97	118.09	113.35	185.58	177.54	140.77	249.95
$\sigma/N/m$	0.010592	0.0093692	0.0088664	0.012149	0.011693	0.0099381	0.011362
Pr	3.7532	2.9141	2.8899	4.4617	4.3796	1.7825	4.1171

top of the evaporator and enters the liquid distributor. Then liquid refrigerant is sprayed onto the horizontal tube’s outer surface to absorb the heat of heating water inside the tube and evaporates. Refrigerant vapor flows back to the condenser and condenses outside the outer surfaces of the tubes in which chilling water flows. It should be noted that the two water tanks can be cooled by the refrigerator and heated by the electrical heater to adjust to the required temperature. And they both have insulation layer to reduce their heat exchange with the environment. Before experiment, the water in the hot water tank and cold water tank should first be cooled to the desired temperature, and during the test the hot water will be further cooled by the vaporization of liquid refrigerant and the cold water will be heated by the condensation of vapor refrigerant. In order to resume to the desired temperature some amount of heat is needed for the hot water tank and some cooling power is needed for the cold water.

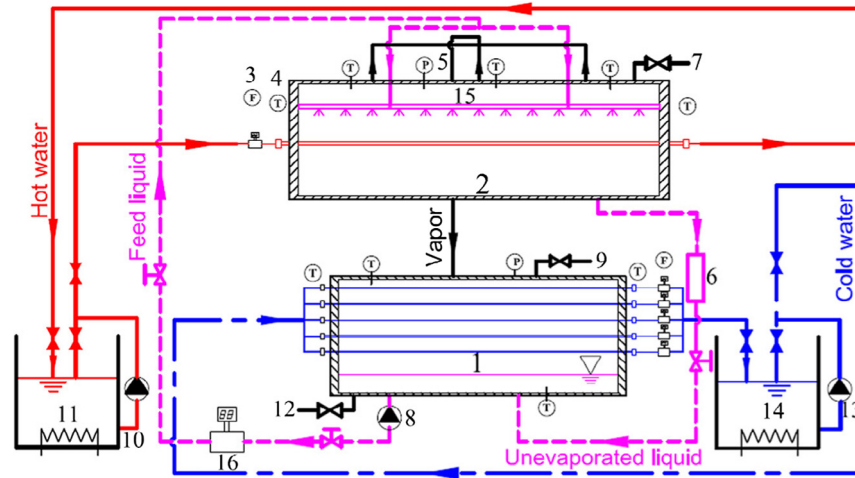
Volume flow rate of heating and chilling water and mass flow rate of liquid refrigerant are measured with electromagnetic flow meter. A digital pressure gauge is employed to measure the pressure in the evaporator. Temperature of liquid refrigerant in the reservoir is measured by platinum resistance thermometer and taken as the saturation temperature. In all data run, the temperature differences between this temperature and that corresponding to the measured pressure of the evaporator is less than 0.1 K. RTDs (resistance temperature detectors) are installed at the inlet and outlet of the water to measure the temperature differences. Specifications of measurement instruments are listed in Table 3.

Liquid distributor used in this test is shown in Fig. 2. It is comprised of two boxes, which serve as a preliminary and a secondary distributor separately. The top plate of the second one is open-ended. The liquid level in the second box varies with liquid flow rate which makes the liquid refrigerant flow under gravity. Two rows of orifices with diameter of 2.0 mm and spacing of 15.0 mm are drilled at the bottom surface of the top box. With the same diameter and pitch, one row of orifices are drilled at the bottom surface of the second box which are in vertical line with the top-most points of the tube. The liquid distributor height is about 6 mm from the bottom surface to the dummy tube (with the same diameter and length as the test tube) which is served as a liquid distributor too. Tube pitch between the dummy tube and the test tube is 25 mm.

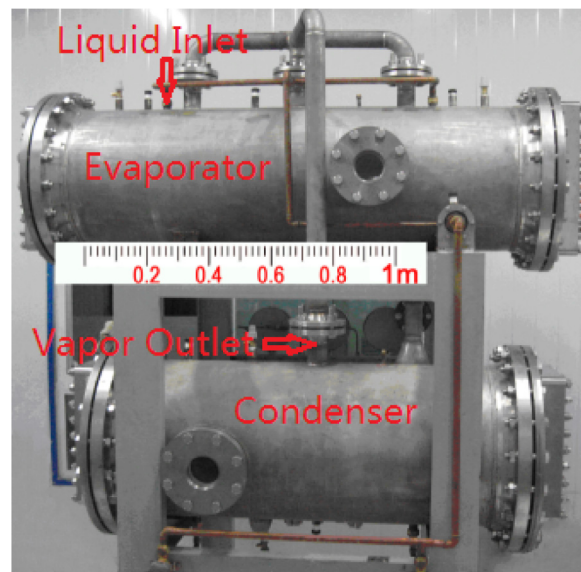
The tube tested is a plain copper tube with outer diameter of 19.05 mm, inner diameter of 17.19 mm and effective length of 1500 mm. The tube on two end plates of the evaporator was fixed with O rings imbedded in the flange. The horizontal position is ensured carefully by a gradienter during the installation of the test section.

2.2. Test procedure

When the installation of the test section have been finished, high-pressure nitrogen is charged into the system until the absolute pressure reaches around 1.2 MPa. Leakage test is satisfied when the pressure loss is less than 1 kPa after 72 h. After that,



1. Condenser (reservoir); 2. Evaporator; 3. Electromagnetic flowmeter; 4. RTDs; 5. Pressure gauge; 6. Condensate measuring container; 7. Exhausting valve; 8. Magnetic Pump; 9. Refrigerant charging valve; 10. Hot water pump; 11. Hot water tank; 12. Refrigerant outlet; 13. Cold water pump; 14. Cold water tank; 15. Liquid refrigerant distributor; 16. Coriolis mass flowmeter
 (a) Diagram of the experimental apparatus



(b) Whole view of the evaporator and condenser

Fig. 1. Diagram and real picture of the experimental apparatus.

Table 3
 Specifications of key measurement instruments.

Instruments	Specification	Precision	Range
Mass flow meter	SIEMENS MASS2100	0.1%	0–5000 kg·h ⁻¹
Volume flow meter	SIEMENS MAGFLO MAG5100W	0.1%	0–3000 L·h ⁻¹
Pressure gauge	KELLER LEX1	0.05%	–0.1 to 2.0 MPa
RTDs	OMEGA Pt100 1/10 DIN	±(0.03 + 0.0005 T) °C	0–60 °C
Data acquisition	Keithley digital voltmeter	0.1 μV	1000 V

the system is evacuated by a vacuum pump until the absolute pressure is no more than 800 Pa. A small quantity of refrigerant is charged into the system first, then evacuated by the vacuum pump until the absolute pressure is less than 800 Pa. This operation should be repeated three times before the final charging of refrigerant.

Before each group of tests, sufficient time (about 2 h) is spent until equilibrium condition is reached for the system. The equilibrium condition is identified by the temperature difference between the refrigerant liquid in the condenser and the one corresponding to the measured pressure in the evaporator, the difference should be less or equal to 0.1 K. For each data run a group of 10 data will

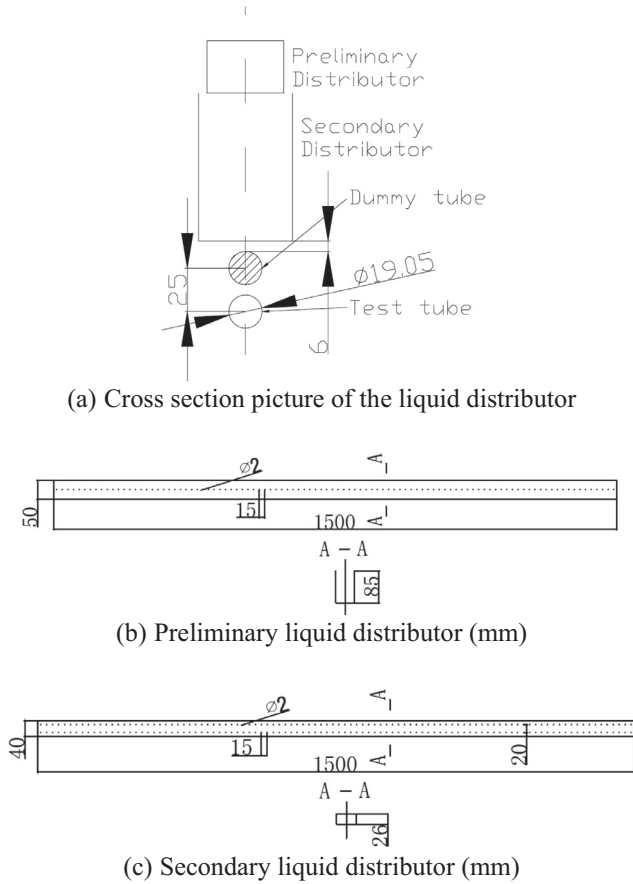


Fig. 2. Diagram of the liquid distributor.

be saved if the fluctuation of the saturation pressure during the data acquisition process is within ± 200 Pa.

During the test, condensate temperature is mainly controlled by adjusting the cooling water temperature flowing in tubes of the condenser to make sure that the saturation temperature measured in the bottom of condenser reaches the desired value. The temperature of the cooling water varied with heat flux under the same saturation temperature but usually was in the range of 1°C below the saturated temperature. In addition, the pressure in the evaporator served as an indicator of the desired saturated temperature.

3. Data reduction method and uncertainty analysis

3.1. Heat transfer rate and heat balance

Heat dissipated by the heating water and absorbed by the chilling water is calculated by Eqs. (1) and (2) respectively:

$$\phi_e = \dot{m}_e c_p (T_{e,\text{in}} - T_{e,\text{out}}) \quad (1)$$

$$\phi_c = \dot{m}_c c_p (T_{c,\text{out}} - T_{c,\text{in}}) \quad (2)$$

where \dot{m}_e and \dot{m}_c are mass flow rate of heating water and chilling water respectively, c_p is the specific heat capacity of water inside the tube.

For all the test data presented in this paper, heat balance deviation is less than 5% as shown in Eq. (3):

$$(\phi_e + \phi_p - \phi_c) / \phi_r \leq 5\% \quad (3)$$

where ϕ_p is the power of the canned motor pump which is immersed in the bulk of liquid refrigerant for pumping the liquid

refrigerant in condenser to the liquid distributor; ϕ_r is the reference heat transfer rate, defined by Eq. (4):

$$\phi_r = (\phi_e + \phi_c + \phi_p) / 2 \quad (4)$$

For the canned motor pump, part of pumped liquid is used to cool the motor and this part of liquid is heated and maybe partially vaporized and then return to the condenser without being carried to the liquid distributor. To verify the reasonability of Eqs. (3) and (4), simple calculation was done. At the largest liquid flow of R134a, 1484 kg/h measured by mass flowmeter, the kinetic energy of the pumped refrigerant liquid is 0.42 W and the gravitational potential power is 7.27 W, the total power carried by the pumped liquid is 7.69 W while the pump power is 874 W. At the lowest flow of R134a, 154 kg/h measured by mass flowmeter, the kinetic energy rate is 0.000468 W and the gravitational potential energy rate is 0.755 W, the total power is 0.756 W while the pump power is 646 W. For the extreme situations no more than 1% of the pump power is converted into the kinetic and gravitational potential energy of the liquid refrigerant. So that all the power of canned pump ϕ_p is added to the input power of the condenser in conjunction with the heating power ϕ_e from the hot water going through the evaporator.

The temperature of the cooling water varied with heat flux under the same saturation temperature but usually was in the range of 1°C below the saturated temperature. For example, at $T_s = 6^\circ\text{C}$, the temperature of the cooling water is about 5.27°C when the heat flux is 60 kW/m^2 , while 5.59°C when the heat flux is 10 kW/m^2 . The ratio between condensate steam and unevaporated liquid in the reservoir is less than 0.5%. For R134a, when the heat flux is 60 kW/m^2 , the rate of condensate production is about 0.02866 kg/s , the unevaporated liquid in the reservoir is about 40 kg , so that the condensate has negligible effect on the temperature of feed liquid.

3.2. Overall heat transfer coefficients

The overall heat transfer coefficients of the tested tube can be expressed by Eq. (5):

$$k = \frac{\phi_e}{A_o \Delta T_{LMTD}} \quad (5)$$

where A_o is the outer surface area of the tube, ΔT_{LMTD} is the logarithm mean temperature difference between water and refrigerant saturation temperature.

ΔT_{LMTD} is defined by Eq. (6):

$$\Delta T_{LMTD} = \frac{(T_{e,\text{in}} - T_{e,\text{out}})}{\ln \left[\frac{(T_{e,\text{in}} - T_{\text{sat}})}{(T_{e,\text{out}} - T_{\text{sat}})} \right]} \quad (6)$$

where T_{sat} is the saturation temperature of the refrigerants.

3.3. Evaporation heat transfer coefficients

The overall thermal resistance can be expressed by Eq. (7):

$$\frac{1}{k} = \frac{1}{h_o} + R_w + R_f + \frac{1}{h_i} \frac{D_o}{D_i} \quad (7)$$

where D_i and D_o are the inner and outer diameter of the tested tube, R_w is the thermal resistance of the tube wall, h_i is the water side convective heat transfer coefficient calculated by Gnielinski correlation [22,23] and R_f is the fouling thermal resistance. Since the tested tubes have been cleaned before installation, fouling thermal resistance can be neglected in this study.

Hence, the falling film evaporation heat transfer coefficient can be determined by Eq. (8):

$$h_o = \left[\frac{1}{k} - \frac{1}{h_i} \frac{D_o}{D_i} - R_w \right]^{-1} \quad (8)$$

It should be noted that the heat transfer coefficient obtained above is the average value of the entire tube. By the thermal resistance separation method no information about the local heat transfer coefficient can be obtained. For engineering design purpose, the average heat transfer coefficient works.

3.4. Heat flux and film Reynolds number

Heat flux in this paper is the area-averaged heat flux on the outer surface of the tube tested:

$$q = \frac{\phi_e}{A_o} \quad (9)$$

where ϕ_e is heat transfer rate of the tested tube, and A_o is the outer surface area of the tested tube.

Film Reynolds number is defined by Eq. (10):

$$Re_f = \frac{4\Gamma}{\mu_1} \quad (10)$$

where Γ is the film flow rate on one side of the tested tube per unit length, μ_1 is the dynamic viscosity of the liquid refrigerant at the specific saturation temperature.

3.5. Uncertainty analysis

First the heat loss from the evaporator to environment was examined. The worst heat loss situation is the one when only the hot water pump is turned on without refrigerant evaporation on the tube outside surfaces. For such situation the maximum deviation of inlet and outlet temperature of hot water is within 0.03 K which shows that the evaporator insulation is very good and its heat loss to the environment can be neglected when determining heat transfer rate from water enthalpy differences.

Uncertainty of calculating Re_f depends on the precision of the mass flow meter (see Table 2), and the uncertainty of μ_1 . As indicated above, the difference between the two temperatures (pressure-corresponding saturation temperature and liquid temperature in reservoir) is within 0.1 °C which suggests that the boiling process is saturation boiling. Hence μ_1 is the dynamic viscosity of the saturated refrigerant. Since the measurement uncertainty of mass flow rate is quite small (about 0.5%), the uncertainty of Re_f is subjected to the uncertainty of dynamic viscosity of liquid refrigerant which is also small (usually less than 2%) [24].

Uncertainty of h_o cannot be estimated directly because the outside thermal resistance was separated from the overall thermal resistance. So the uncertainties of h_o is estimated using the method suggested in [25–29]. The estimated uncertainties of k are less than 3.5% for all test conditions. The accuracy for determining heat transfer coefficient on the tube side is quoted to be within 10% [30]. For all experimental data, the percentage of water side thermal resistance varied from 22% to 61%. Results of uncertainty

analysis for h_o are shown in Table 4, and the maximum uncertainty of h_o is less than 15%.

4. Experimental results

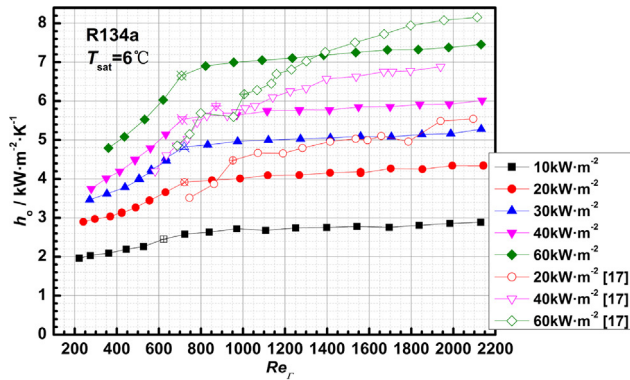
Effects of several influencing parameters (heat flux, saturation temperature and film Reynolds number) on heat transfer performance are investigated and analyzed in this section.

Falling film evaporation heat transfer coefficients versus film Reynolds number of R134a, R290 and R600a at two saturation temperatures are shown in Fig. 3. In Fig. 3(b) and (c) each curve is characterized by two numbers, the 1st one is the saturation temperature and the second represents heat flux. First the results for R134a are analyzed. It can be seen that each curve exhibits two stages, a quasi-plateau stage and a sharp decrease stages. This phenomenon is more obvious for higher heat flux. This variation trend agrees well with previous results, say [7,17]. The sharp decrease stage after the turning point are caused by partial dryout at the tube’s outer surface. The dryout at low film flow rate may be resulted from three aspects. The first one is the uneven distribution of liquid refrigerant at lower film flow rate. Because the distributor is working under gravity, when the liquid flow rate is small, the liquid layer thickness in the secondary box (distributor) is quite thin, and the instability of the free surface may cause great liquid flow rate fluctuation among different holes along the tube length. The second one lies in the different local heat transfer condition along the tube length. Water at the inlet owns a higher temperature and higher local heat transfer coefficient, leading to a higher local heat flux and evaporation rate. If the supply of liquid refrigerant cannot compensate the evaporated one, dryout may happen near the inlet area first. Last point may be rooted in the nucleate boiling heat transfer mechanism. Bubbles induced on the tube surface must escape through the falling film which may break the continuous thin liquid film at lower film Reynolds number. Methods for determining the threshold film Reynolds proposed in [17] is employed, and thus obtained threshold film Reynolds numbers are marked by adding a cross symbol onto the original data point for each curve. It can be seen that such determined threshold Re_f ranges from 600 to 750 under five heat fluxes from small to large. Fig. 3(a) also show that in the two stages heat flux can appreciably enhance heat transfer. This variation trend of h_o vs q is the same for R290 and R600a and will be further discussed in Fig. 4. It is to be noted that the data for R134a at $T_s = 6$ °C in Fig. 3 and in [17] were measured at the same test system, but they do not coincide exactly. The average root-mean-square deviation is 6.85%. Considering the uncertainty of h_o measurement is about 15%, the deviation is acceptable.

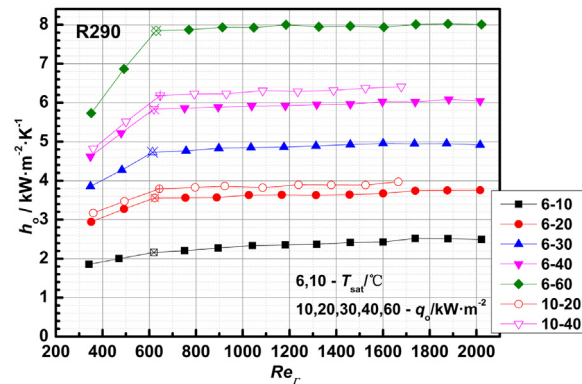
Second, the data for R290 are investigated. Similar trend can be observed, and the threshold film Reynolds numbers determined according to [17] are about 600–650 which are close to those of R134a because of their similar thermo-physical properties. Apart from the similarities, curves are much flatter at the quasi-plateau stage for R290. HTC’s are slightly higher when saturation temperature is 10 °C than those of 6 °C under the two heat fluxes (20 and 40 kW/m²) tested.

Table 4
Experimental measurement uncertainties of overall and falling film heat transfer coefficients.

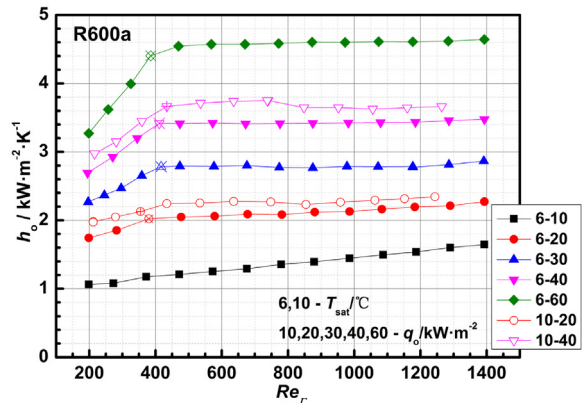
D_o /mm	T_{sat} /°C	q_o /kW·m ⁻²	Uncertainty of k	Uncertainty of h_o
19.05	6	10	4.25%	14.2%
		20	3.18%	13.3%
		30	3.17%	13.1%
		40	3.17%	13.8%
		60	3.16%	12.3%
		10	20	3.08%
		40	3.10%	13.0%



(a) R134a



(b) R290



(c) R600a

Fig. 3. Variation of HTCs versus film Reynolds number for R134a, R290 and R600a.

Finally data for R600a are examined. As it can be seen in the figure, two stages with decreasing film Reynolds number can be distinguished for each curve except when the heat flux is $10 \text{ kW}\cdot\text{m}^{-2}$ where HTCs decrease almost linearly with film Reynolds number within the range tested. This may result from the dominance of convective heat transfer at lower heat flux. Threshold film Reynolds number varies around 400 within the heat fluxes tested. The same as R290, increase of saturation temperature will benefit the heat transfer coefficient gently.

Fig. 4 shows the variation trend of HTCs versus heat flux for the three working fluids, for each refrigerant, tests are conducted under two film Reynolds numbers.

For R134a, three regimes can be clearly observed which are separated by heat flux of $10 \text{ kW}\cdot\text{m}^{-2}$ and $110 \text{ kW}\cdot\text{m}^{-2}$. HTC increases mildly under $10 \text{ kW}\cdot\text{m}^{-2}$, then almost linearly in the log–log

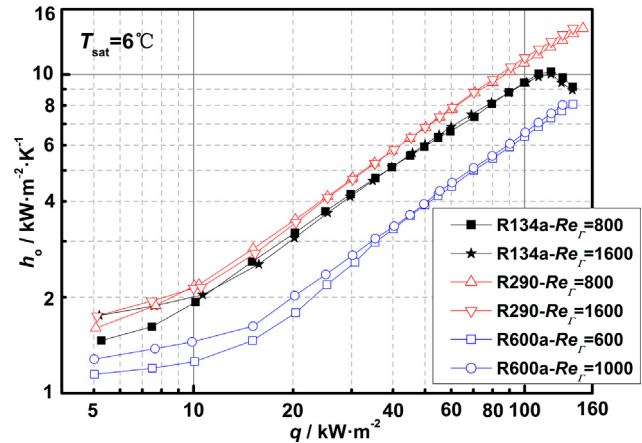


Fig. 4. Variation of HTCs versus heat flux for R134a, R290 and R600a.

coordinate between $10 \text{ kW}\cdot\text{m}^{-2}$ and $110 \text{ kW}\cdot\text{m}^{-2}$, after that, it drops with the further increase of heat flux because of the appearance of partial dryout. Such variation trend of h_o vs q can be explained by three heat transfer mechanisms, convective heat transfer dominates at lower heat fluxes, while nucleate boiling heat transfer dominates at higher ones (in this region $h_o \propto q^n$) and after that region dryout occurs. In addition, when heat flux is lower than $10 \text{ kW}\cdot\text{m}^{-2}$, higher HTCs are achieved with a larger film Reynolds number, while in the nucleate boiling-dominated region, similar HTCs are obtained with two Re_f . This kind of h_o vs q curve variation is somewhat similar to that of the pool boiling curve.

As for R290 and R600a, generally their variation trend of h_o vs q are more or less the same as R134a, with following three differences. First, decrease of HTCs is not observed under high heat flux more than $110 \text{ kW}\cdot\text{m}^{-2}$. Second, at lower heat flux, HTCs of R290 under the two film Reynolds numbers are much closer than those of R134a. Third, for R600a, the convection dominated region extends to heat flux of $20 \text{ kW}\cdot\text{m}^{-2}$. This phenomenon suggests that the incipient of nucleate boiling for R600a is much later than those of R134a and R290. As a whole, R290 exhibits highest HTCs among the three refrigerants especially at higher heat fluxes, and R600a the smallest.

5. Empirical heat transfer correlations for single smooth tube

In this part, new heat transfer correlations are suggested based on the data of five refrigerants not only from this paper but also from two references [20,21] under two regimes (fully wetting and dryout) separated by Re_{thr} respectively, and their prediction results are compared with the present data as well as data in previous literature. Thermo-physical properties of all refrigerants are determined from Ref. [24].

5.1. Determination of the threshold film Reynolds number (Re_{thr})

As indicated above, the variation curves of HTC with film Reynolds number are used to calibrate the threshold film Reynolds number. HTCs at turning points (Re_{thr}) from full wetting to partial dryout regime are 8%–10% lower than the average value of HTCs at larger film Reynolds numbers of the curve. Methods employed to determine the Re_{thr} are described in detail in Ref. [17]. The threshold film Reynolds numbers are marked with an additional cross symbol as shown in Fig. 3. Data at turning points are used at both full wetting and partial dryout regimes to obtain the correlations. What should be pointed out here is that data at saturation

temperature of 6 °C and heat flux of 10 kW·m⁻² for R600a are all taken as the full wetting condition.

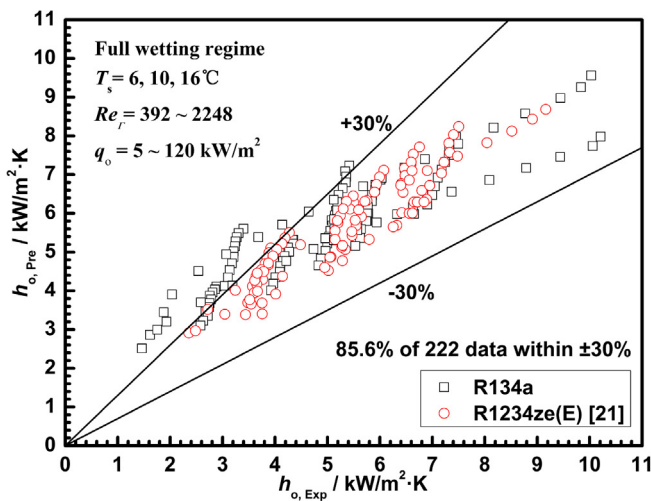
5.2. Comparison between previous correlations and the present data base

As indicated above, correlations suggested by Zhao et al. [17] (later for simplicity, just Zhao et al.s' correlation) can fit the experiment data from several other references well for different refrigerants (R22, R141b and R245fa, etc.) despite the fact that Zhao et al. s'correlations are correlated based of the data of R134a. Furthermore, Ref. [7] shows that Zhao et al.s' correlations achieve success in predicting HTC's of R134a and R123 on a horizontal smooth tube. Therefore, in this part, the present data base is first compared with Zhao et al.s' correlations. As shown in Fig. 5(a) and (b), Zhao et al.s' correlations [17] fits the data for R134a and R1234ze(E) quite well, with 85.6% of 222 data within the deviation of ±30% under full wetting regime and with 99% of 104 data within the deviation of ±30% under partial dryout regime. This is because the properties of R1234ze(E) is quite close to those of R134a. However, from Fig. 5 (c) and 5(d), we can see the correlations overpredict the heat

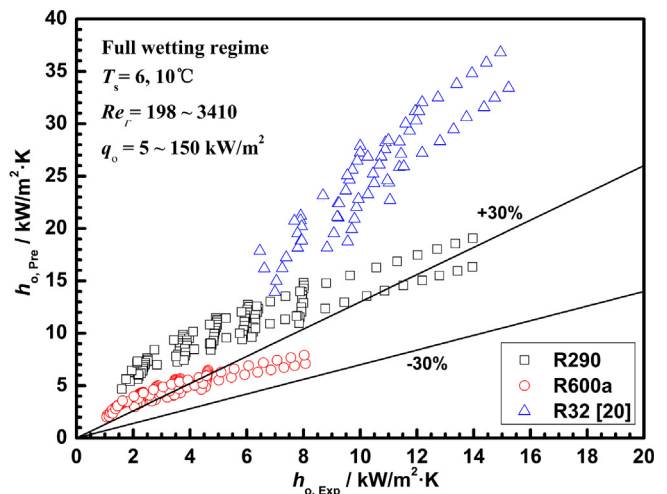
transfer coefficient with a large deviation for most of the data of R600a, R290 and R32. Under full wetting regime, deviation of most data is beyond 30%, and under dryout regime, only 62.1% of 58 data within the deviation of ±30%. The significant deviation of the HTC's between prediction results and experimental results of R32 may be partially attributed to the big difference in the Prandtl number. The Prandtl number of Zhao et al.s' correlation [17] is from 3.4 to 4.25 while that of R32 is only 1.78. This comparison implies that it is not able to adopt Zhao et al.s' correlations [17] to represent all our test data. An improved one is needed.

5.3. Dimensionless analysis and correlating method

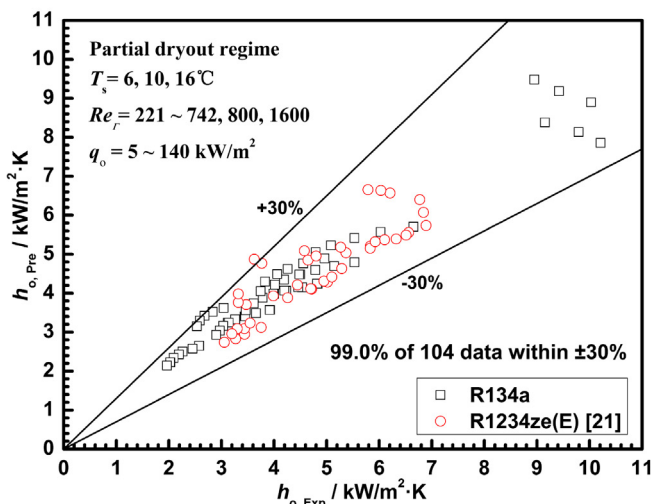
In order to create an improved correlation, the dimensional analysis method is adopted to obtain the related dimensionless numbers for the falling film heat transfer prediction. According to the present experimental conditions, the heat transfer coefficient h_o could be influenced by heat flux q , film flow rate Γ , saturation temperature T_{sat} and thermo-physical properties of working fluids. Since contact angle between refrigerant and copper surface is very small (usually less than 2.5°) according to Ref. [31] and our



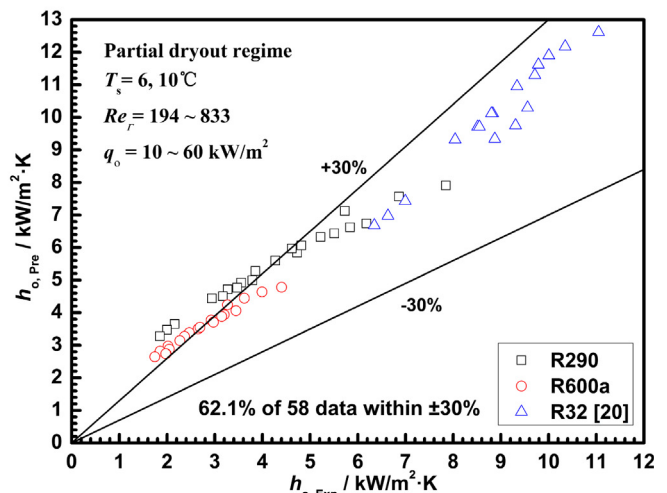
(a) R134a and R1234ze(E) at full wetting regime



(c) R290, R600a and R32 at full wetting regime



(b) R134a and R1234ze(E) at partial dryout regime



(d) R290, R600a and R32 at partial dryout regime

Fig. 5. Predicted h_o using correlations of Zhao et al. [17] against the present data base.

observation on the liquid film which is continuous most of the time, the effect of surface tension on falling film heat transfer can be neglected. From the dimensionless analysis, following well known dimensionless numbers can be derived to express the heat transfer prediction correlations:

$$\begin{aligned} \text{Nusselt number } Nu &= h_o D_o / \lambda_i; \\ \text{Film Reynolds number } Re_\Gamma &= 4\Gamma / \mu_i; \\ \text{Prandtl number } Pr &= \mu_i c_{p,i} / \lambda_i; \text{ and} \\ \text{Boiling number } Bo &= q D_o / r \Gamma. \end{aligned}$$

The basic form of heat transfer correlations is expressed as follows:

$$Nu = a Re_\Gamma^{b1} Bo^{b2} Pr^{b3} \quad (11)$$

To enlarge the range of the correlation applicability, the original experimental data of falling film evaporation of R32 and R1234ze (E) outside a single horizontal tube from [20,21] are taken as the data base together with the present data. Totally 542 and 162 test data are adopted for the full wetting and partial dryout regimes, respectively.

By regression analysis, the values of a and $b1$ – $b3$ are obtained as shown in Eq. (12).

5.4. Heat transfer correlations for two regimes

For the full wetting regime, the correlated equation is:

$$Nu = 23.3 Re_\Gamma^{0.8174} Bo^{0.6331} Pr^{-0.0864} \quad (12)$$

$$\begin{aligned} \text{For: } Re_\Gamma &= 3.92 \times 10^2 - 3.5 \times 10^3 \\ Bo &= 5.16 \times 10^{-3} - 3.30 \times 10^{-1} \\ Pr &= 1.77 - 4.46 \end{aligned}$$

It may be noted that under full wetting condition, most of the data is within the nucleation boiling dominated regime (more than 95%) and the correlations suggested above can be used to predict the heat transfer coefficient in this regime with reasonable accuracy.

For the partial dryout regime, following equation is obtained:

$$Nu = 11.7 Re_\Gamma^{0.8931} Bo^{0.5278} Pr^{-0.0287} \quad (13)$$

$$\begin{aligned} \text{For } Re_\Gamma &= 1.95 \times 10^2 - 8.33 \times 10^2 \\ Bo &= 2.2 \times 10^{-2} - 3.56 \times 10^{-1} \\ Pr &= 1.77 - 4.46. \end{aligned}$$

We can see from the correlations that the exponent of film flow rate Γ is 0.1843 and 0.3653 for the full wetting and partial dryout regimes respectively, and this corresponds well with the results in Fig. 3 where HTC is more sensitive to film Reynolds number at partial dryout regime.

Deviation between correlation-prediction and experimental data base for both full wetting and partial dryout regimes are shown in Fig. 6(a) and (b) respectively. For the full wetting regime, 96.7% of all the 542 data are within $\pm 30\%$; for the partial dryout regime, 97.5% of all the 162 data are within $\pm 30\%$.

Comparison with data in other references are exhibited in Fig. 7. For the full wetting regime, deviation of 73.4% of 289 data ranges from -30% to $+15\%$. Highest deviation occurs at lower heat fluxes where the uncertainty in heat flux measurement may be relatively large. For the partial dryout regime, deviation of 76.8% of 95 data within $\pm 30\%$. It is worth noting that all the original data for smooth tube in [7,17] are compared in Fig. 7, and it can be seen that the

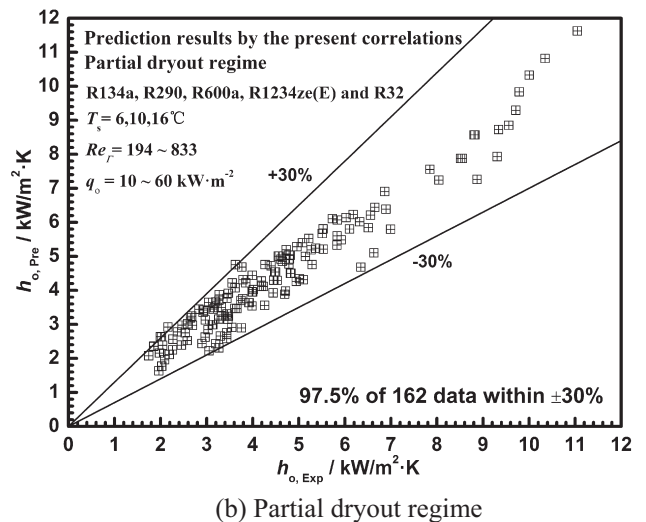
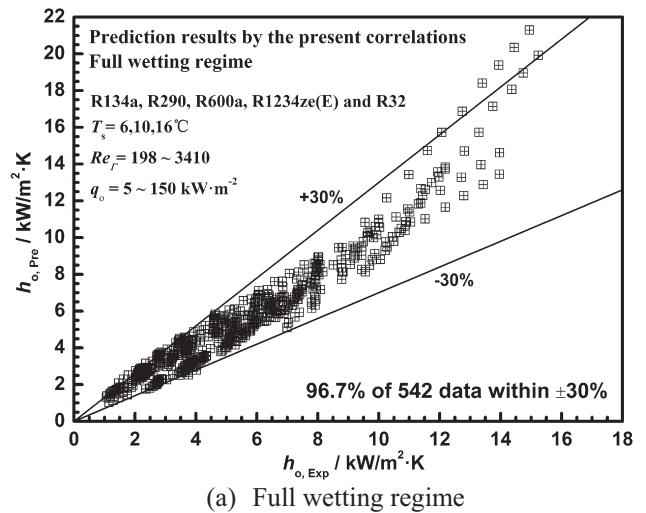
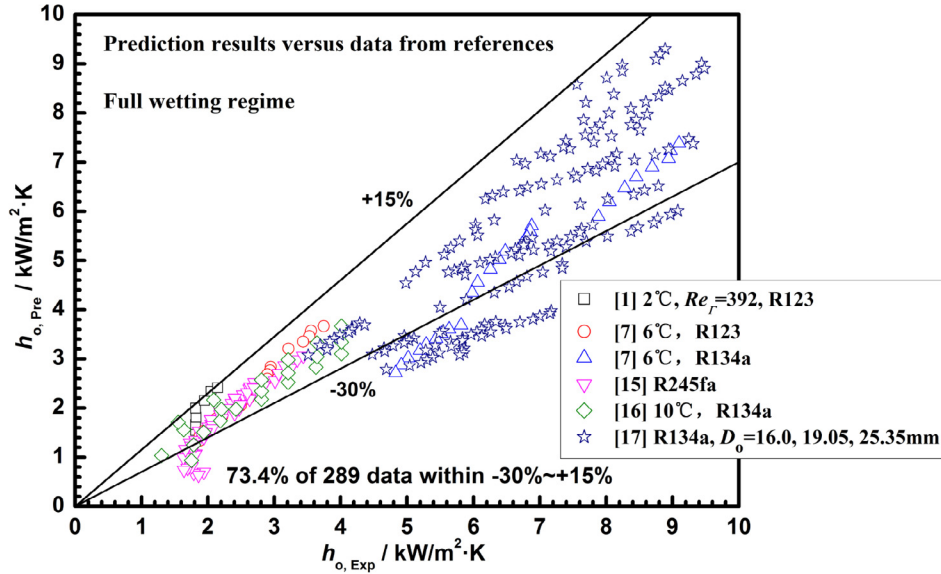


Fig. 6. Comparison of h_o between correlation-prediction and experimental data base.

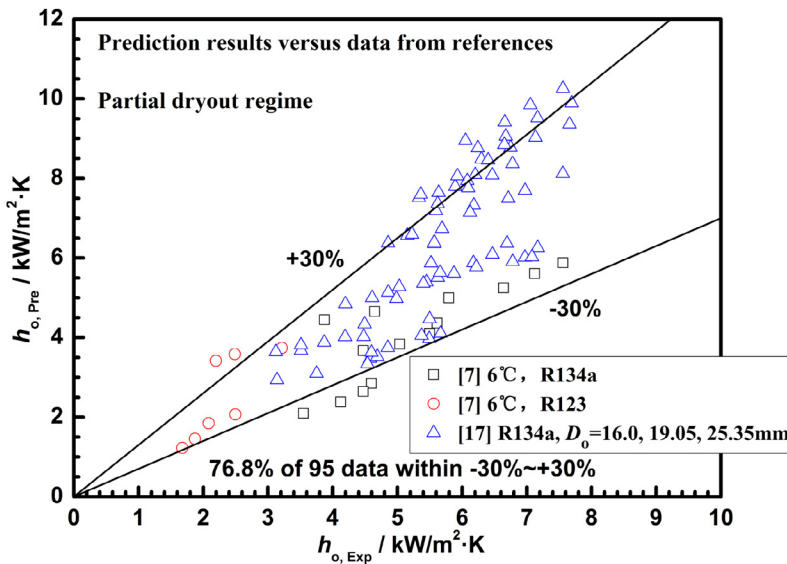
agreements are quite good, even though a bit worse than the agreement between them and Zhao et al.'s correlations. As indicated above that in Eqs. (12) and (13), the exponent of film flow rate Γ in the full wetting regime is less than that in the partial dryout regime which is in accordance with the test data; while in Zhao et al.'s correlations the exponent of the full wetting regime is a bit larger than that of the partial dryout regime (0.26 vs 0.18) which is physically inappropriate.

It should be noted that all the compared test data of [1,15,16] shown in Fig. 7 were obtained from the figures in the published papers since we have no way to get the original test data. Even though modern technical software can quite accurately read the values from figure about 5% uncertainty of data reading should be considered. As proposed in [17] that reliable data accumulation is very important in order to establish a well-accepted general correlation. Our test data of this paper will be uploaded in our group website once this paper is accepted. And we once again appeal other researchers to do so in order to avoid the additional reading errors from paper figures.

Finally, it is noted here that what has been presented above is the averaged heat transfer coefficient which is useful for the engineering design, but is lack of physical mechanism details. Modern measurement methods for the wall temperature distribution on



(a) Full wetting regime



(b) Partial dryout regime

Fig. 7. Comparison of h_o between prediction results of the present empirical correlations and experimental results from Refs. [1,7,15,16,17].

pipe, as well as measuring methods for film thickness, wave characteristics, and so on are needed. With such data, it is possible to understand this complicated heat transfer process from physical point of view and may lead to a more general and accurate prediction correlation. This can be regarded as the further research needs in this regard.

6. Conclusion

Several conclusions can be drawn based on the present study:

1. The effect of heat flux on falling film evaporation heat transfer is always positive in both full wetting and partial dry-out regimes for the conditions tested.
2. Heat transfer performance of R600a is inferior than R134a under the tested conditions, while R290 owns slightly higher HTC than those of R134a.
3. The way for determining the threshold Reynolds number suggested by Zhao et al. [17] is adopted to delineate the variation curve into full wetting and partial dryout regimes and such determined threshold film Reynolds number is 600–700 for R134a, 600–650 for R290 and around 400 for R600a except for the case of $T_{\text{sat}} = 6\text{ }^\circ\text{C}$ and $q = 10\text{ kW}\cdot\text{m}^{-2}$.
4. Two correlations for five refrigerants are constructed based on the present test data and data from Refs. [20,21]. The correlation for full wetting regime fits 96.7% of the total 542 correlated data within $\pm 30\%$ while fits 73.4% of the total 289 data from other papers from -30% to $+15\%$, the correlation for partial

dryout regime fits 97.5% of the total 162 correlated data within $\pm 30\%$ while fits 76.8% of the total 95 data of other references within $\pm 30\%$.

Conflict of interest

No conflict of interest needs to be declared.

Acknowledgement

This work was supported by the Foundation for Innovative Research Groups of the National Natural Science Foundation of China (No. 51721004) and 111 Project (B16038).

References

- [1] S.A. Moeykens, Heat Transfer and Fluid Flow in Spray Evaporators with Application to Reducing Refrigerant Inventory (Ph.D. thesis), Iowa State University, Iowa, USA, 1994.
- [2] J.F. Roques, J.R. Thome, Falling films on arrays of horizontal tubes with R-134a, Part I: boiling heat transfer results for four types of tubes, *Heat Transfer Eng.* 28 (5) (2007) 398–414.
- [3] M. Habert, J.R. Thome, Falling-film evaporation on tube bundle with plain and enhanced tubes—Part I: Experimental results, *Exp. Heat Transfer* 23 (4) (2010) 259–280.
- [4] M. Christians, J.R. Thome, Falling-film evaporation on enhanced tubes, part 1: experimental results for pool boiling, onset-of-dryout and falling film evaporation, *Int. J. Refrig.* 35 (2012) 300–312.
- [5] Wen-Tao Ji, Chuang-Yao Zhao, Ding-Cai Zhang, et al., Effect of vapor flow on the falling film evaporation of R134a outside a horizontal tube bundle, *Int. J. Heat Mass Transf.* 92 (2016) 1171–1181.
- [6] C.Y. Zhao, W.T. Ji, P.H. Jin, et al., Cross vapor stream effect on falling film evaporation in horizontal tube bundle using R134a, *Heat Transfer Eng.* (2017) 1–14.
- [7] C.Y. Zhao, P.H. Jin, W.T. Ji, et al., Experimental investigations of R134a and R123 falling film evaporation on enhanced horizontal tube, *Int. J. Refrig.* 75 (2017) 190–203.
- [8] C.Y. Zhao, W.T. Ji, P.H. Jin, et al., Experimental study of the local and average falling film evaporation coefficients in a horizontal enhanced tube bundle using R134a, *Appl. Therm. Eng.* 129 (2018) 502–511.
- [9] J. Fernández-Seara, Á.Á. Pardiñas, Refrigerant falling film evaporation review: description, fluid dynamics and heat transfer, *Appl. Therm. Eng.* 64 (2014) 155–171.
- [10] A.M. Abed, M.A. Alghoul, M.H. Yazdi, et al., The role of enhancement techniques on heat and mass transfer characteristics of shell and tube spray evaporator: a detailed review, *Appl. Therm. Eng.* 75 (2015) 923–940.
- [11] G.N. Danilova, V.G. Burkin, V.A. Dyundin, Heat transfer in spray-type refrigerator evaporators, *Heat. Transf. Sov. Res.* 8 (1976) 105–113.
- [12] Y. Fujita, M. Tsutsui, Experimental investigation of falling film evaporation on horizontal tubes, *Heat. Transf. Jpn. Res.* 27 (1998) 609–618.
- [13] G. Ribatski, J.-R. Thome, Experimental study on the onset of local dryout in an evaporating falling film on horizontal plain tubes, *Exp. Therm. Fluid Sci.* 31 (2007) 483–493.
- [14] L.H. Chien, C.H. Cheng, A predictive model of falling film evaporation with bubble nucleation on horizontal tubes, *HVAC&R Res.* 12 (1) (2006) 69–87.
- [15] L.H. Chien, Y.L. Tsai, An experimental study of pool boiling and falling film vaporization on horizontal tubes in R-245fa, *Appl. Therm. Eng.* 31 (2011) 4044–4054.
- [16] L.H. Chien, R.H. Chen, An experimental study of falling film evaporation on horizontal tubes using R-134a, *J. Mech.* 28 (2) (2012) 319–327.
- [17] C.Y. Zhao, W.T. Ji, P.H. Jin, et al., Heat transfer correlation of the falling film evaporation on a single horizontal smooth tube, *Appl. Therm. Eng.* 103 (2016) 177–186.
- [18] A.A. Alhusseni, K. Tuzla, J.C. Chen, Falling film evaporation of single component liquids, *Int. J. Heat Mass Transf.* 41 (12) (1998) 1623–1632.
- [19] M.G. Cooper, Saturation nucleate pool boiling—a simple correlation, *Int. Chem. Eng. Symp. Ser.* 86 (1984) 785–792.
- [20] P.H. Jin, C.Y. Zhao, W.T. Ji, et al., Experimental investigation of R410A and R32 falling film evaporation on horizontal enhanced tubes, *Appl. Therm. Eng.* 137 (2018) 739–748.
- [21] P.H. Jin, Z. Zhang, I. Mostafa, et al., Low GWP refrigerant R1234ze(E) falling film evaporation on a single horizontal plain tube and enhanced tubes with reentrant cavities, *Proceedings of the 9th Asian Conference on Refrigeration and Air Conditioning*, Sapporo, Japan, 2018.
- [22] V. Gnielinski, New equations for heat and mass transfer in the turbulent flow in pipes and channels, *Int. Chem. Eng.* 16 (1976) 359–368.
- [23] V. Gnielinski, On heat transfer in tubes, *Int. J. Heat Mass Transf.* 63 (2015) 134–140.
- [24] E.W. Lemmon, M.L. Huber, M.O. McLinden, Reference Fluid Thermodynamic and Transport Properties (REFPROP) Version 8.0, National Institute of Standards and Technology (NIST), 2008.
- [25] S.M. Yang, W.Q. Tao, *Heat Transfer*, fourth ed., Higher Education Press, Beijing, China, 2006.
- [26] S.J. Kline, F.A. McClintock, Describing uncertainties in single-sample experiments, *Mech. Eng.* 75 (1953) 3–9.
- [27] B. Cheng, W.Q. Tao, Experimental study of R-152a film condensation on single horizontal smooth tube and enhanced tubes, *ASME J. Heat Transfer* 116 (1994) 266–270.
- [28] D.C. Zhang, Experimental and numerical investigation of refrigerant condensation and boiling heat transfer characteristics on doubly-enhanced tubes (Ph.D. thesis), School of Energy and Power Engineering, Xi'an Jiaotong University, 2007.
- [29] Wen-Tao Ji, Ding-Cai Zhang, Ya-Ling He, et al., Prediction of fully developed turbulent heat transfer of internal helically ribbed tubes – an extension of Gnielinski equation, *Int. J. Heat Mass Transf.* 55 (2012) 1375–1384.
- [30] Y.A. Cengel, A.J. Ghajar, Chapter eight: internal forced convection, in: *Heat and Mass Transfer, Fundamentals and Applications*, McGraw-Hill, New York, 2011, p. 489.
- [31] Lu. Xingbin, Jinping Liu, Xu. Xiongwen, Contact angle measurements of pure refrigerants, *Int. J. Heat Mass Transf.* 102 (2016) 877–883.